Available online at www.sciencedirect.com
SCIENCE DIRECT®
Journal of Organometallic Chemistry 690 (2005) 2679–2687
Journal of Organometallic Chemistry
www.elsevier.com/locate/jorganchem

Molecular interactions of nitrogen-containing bisphosphonates within farnesyl diphosphate synthase

Frank H. Ebetino [a,*], Christian N. Rozé [b], Charles E. McKenna [b], Bobby L. Barnett [a], James E. Dunford [c], R. Graham G. Russell [d], Glen E. Mieling [a], Michael J. Rogers [c]

[a] *Procter & Gamble Pharmaceuticals, Mason, OH 45040, USA*
[b] *Department of Chemistry, University of Southern California, Los Angeles, CA 90089-0744, USA*
[c] *Department of Medicine and Therapeutics, University of Aberdeen, Aberdeen AB25 2ZD, UK*
[d] *The Botnar Research Centre and Oxford University Institute of Musculoskeletal Sciences, Nuffield Department of Orthopaedic Surgery, Nuffield Orthopaedic Centre, Headington, Oxford OX3 7LD, UK*

Received 28 January 2005; accepted 11 March 2005

Abstract

Bisphosphonates, known for their effectiveness in the treatment of osteoporosis, inhibit bone resorption via mechanisms that involve binding to bone mineral and cellular effects on osteoclasts. The major molecular target of nitrogen-containing bisphosphonates (N-BPs) in osteoclasts is farnesyl diphosphate synthase (FPPS). N-BPs likely inhibit this enzyme by mimicking one or more of the natural isoprenoid lipid substrates (GPP/DMAPP and IPP) but the mode of inhibition is not established. The active site of FPPS comprises a subsite for each substrate. Kinetic studies with recombinant human FPPS indicate that both potent (risedronate) and weak (NE-58051) enzyme inhibitors compete with GPP for binding to FPPS, however, binding to this site does not completely explain the difference in potency of the two inhibitors, suggesting that a second binding site may also be a target of bisphosphonate inhibition. Using the docking software suite Autodock, we explored a dual inhibitor binding mode for recombinant human FPPS. Experimental support for dual binding is suggested by Dixon plots for the inhibitors. N-BPs may inhibit by binding to both the GPP and a second site with differences in potency at least partly arising from inhibition at the second site.

Keywords: Bisphosphonate; Farnesyl diphosphate synthase; Docking; Enzyme kinetics; Dual site inhibition; Risedronate

1. Introduction

Bisphosphonates are currently used to treat postmenopausal and steroid-induced osteoporosis, Paget's disease, hypercalcemia and osteolysis associated with multiple myeloma and metastatic cancers [1–4]. Due to their ability to bind calcium ions in a multidentate manner, bisphosphonates rapidly accumulate in bone [5] where they inhibit the activity of bone-destroying osteoclasts. The antiresorptive activity of the potent nitrogen-containing bisphosphonates (N-BPs) results from two key properties [6], their affinity for bone mineral, and their potency for inhibiting a molecular target in osteoclasts. It has recently been demonstrated [7] that the relative mineral affinity of several clinically utilized bisphosphonates increases in the order etidronate < risedronate < alendronate < zoledronate. The lack of correlation between mineral affinity and antiresorptive potency, (for example, the lower mineral affinity but higher potency of risedronate versus the higher affinity

* Corresponding author. Tel.: +1 513 622 3630; fax: +1 513 622 5343.
E-mail address: ebetino.fh@pg.com (F.H. Ebetino).

0022-328X/$ - see front matter © 2005 Published by Elsevier B.V.
doi:10.1016/j.jorganchem.2005.03.005

but lower potency of alendronate) provides some of the evidence supporting the involvement of cellular targets.

It is now clear that farnesyl diphosphate synthase (FPPS), an enzyme of the mevalonate pathway, is the major enzyme target of N-BPs [8,9] and is inhibited by nanomolar concentrations of these compounds. Furthermore, there is a highly significant correlation between the order of potency for inhibiting human FPPS in vitro and anti-resorptive potency in vivo, with zoledronate and minodronate being extremely potent inhibitors of FPPS. Importantly, minor modifications to the structure and conformation of the side chain that were known to affect anti-resorptive potency have also now been shown to affect the ability to inhibit FPPS. These observations have helped explain the relationship between N-BP structure and anti-resorptive potency. The high degree of evolutionary conservation of this enzyme can explain why N-BPs also inhibit the growth of *Dictyostelium* [10] and other eukaryotic microorganisms such as *Leishmania* [11,12] and *Trypanosome* parasites, by inhibiting FPPS.

The exact mechanism by which N-BPs inhibit FPPS remains unclear. Computer modeling [10] suggests that N-BPs mimic the structure of the enzyme's natural isoprenoid pyrophosphate substrates, geranyl pyrophosphate (GPP)/dimethylallyl pyrophosphate (DMAPP) or act as carbocation transition state analogs [13]. We have previously noted that modeling in the GPP pocket of compounds with dramatic differences in potency does not adequately explain binding differences [14]. Recent X-ray crystallographic studies of *E. coli* FPPS [15] demonstrate binding of risedronate to the GPP/DMAPP substrate pocket with the side chain positioned in the hydrophobic cleft that normally accommodates an isoprenopid lipid, and the phosphonate groups bound to three magnesium ions. However, the conclusions based on these studies must be tempered by three considerations. Firstly, the authors incubated FPPS with an equimolar solution of IPP and risedronate, which may not be representative of pharmacological concentrations in vivo. Secondly, the positively charged, N-methyl analog of risedronate [16,17] cannot undergo equivalent stabilization at the GPP site because its nitrogen is not a hydrogen bond acceptor, yet is more potent (LED = 0.0001 mg/P/kg) than risedronate. Thirdly, extrapolation of the structural results from the *E. coli* enzyme to the human enzyme must be interpreted with caution pending an X-ray crystal structure of the human enzyme.

In this work, we used Autodock to examine the binding modes of the N-BP risedronate and a less potent but structurally similar analog, NE-58051, in both the GPP site and a second site of FPPS derived from a human homology model, based on X-ray crystallographic coordinates from the avian enzyme. We also present supporting results from a preliminary enzyme inhibition kinetics study on recombinant human FPPS.

2. Results and discussion

2.1. The inhibitors

We chose to study a pair of N-BP analogs whose anti-resorptive activities differ greatly to circumvent the potential for misleading conclusions due to minor differences in bone mineral affinity. The selected pair was the clinically useful anti-osteoporosis drug risedronate (in vivo lowest effective dose (LED) = 0.0003 mg/P/kg) and its much less potent homomethylene analog, NE-58051 (LED = 1.0 mg/P/kg, Fig. 1) [8].

It has been postulated that risedronate inhibits FPPS by binding in the GPP binding site [18–21]. The X-ray crystal structure of the risedronate – *E. coli* FPPS complex shows that the bisphosphonate moiety of risedronate is strongly bound to three magnesiums [15]. Additionally, a hydrogen bond is found between the pyridyl nitrogen of risedronate and a threonine in the GPP binding site. This threonine is conserved in the human FPPS. NE-58051, having an additional methylene unit between its pyridyl and bisphosphonate parts, would be unable to form such a hydrogen bond. However, on the basis of previous molecular modeling [14], we found that NE-58051 can fit the large GPP binding site with a similar bisphosphonate–magnesium ion complex. NE-58051 is a much weaker FPPS inhibitor than risedronate (risedronate IC_{50} = 0.01 μM; NE-58051 IC_{50} = 2.93 μM) [8]. When a tight bisphosphonate–magnesium complex is formed, it is unlikely that the loss of one hydrogen bond in the GPP site can account for the 300-fold loss of inhibitory activity of NE-58051 with respect to risedronate. An explanation for this discrepancy was sought by examining interactions of the two inhibitors with an adjacent subsite.

2.2. Molecular modeling of the human enzyme

The X-ray crystal structure of FPPS has been reported for the avian liver enzyme (avFPPS). A sequence alignment shows 66.2% identity between human [22] and avian [23] FPPS. We constructed a homology model of the human FPPS (hhFPPS) based on the X-ray structure

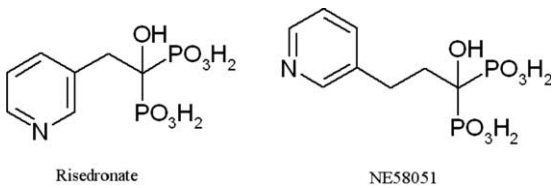

Fig. 1. Risedronate and NE58051.

of the avian liver FPPS (see Section 4). An early precedent for this human FPPS model was our initial ability to explain the bisphosphonate SAR by modeling the bisphosphonates in an adjacent site of the avian structure (Fig. 2) [14]. In this model, a protonated pyridine nitrogen was found to have an important electrostatic interaction with a GPP phosphate. This interaction is consistent for all of the highly potent nitrogen-containing bisphosphonates, including the positively charged N-methyl analog of risedronate. Although the pKa of pyridine is known to be lower than that necessary for protonation at physiological pH, there are many examples in binding pockets of proteins where the environment creates a local pH that is different from bulk pH, e.g., aspartic acid proteases in which the active site aspartates are protonated at pH ranges near neutral [24].

We then conducted a series of docking experiments using a force-field based scoring function with an evolutionary search algorithm as implemented in Autodock 3.05. We were first interested in the possibility of docking a bisphosphonate molecule in a second site with a GPP molecule bound to the GPP site. The enzyme has two DDxxD motifs which are conserved. The first motif chelates a pair of magnesium ions which in turn bind the pyrophosphate moiety of GPP as seen in the avian X-ray crystal structure. We hypothesize that the second aspartate-rich DDxxD motif also binds a pair of magnesium ions that can readily accept a diphosphate or a bisphosphonate molecule.

While this work was in progress, an X-ray crystal structure of *E. coli* FPPS [15] was published. The structure shows different binding modes for dimethylthiodiphosphate (DMSPP), a non-hydrolysable DMAPP substrate analog, IPP and risedronate. DMSPP binds to the GPP site with three magnesium ions surrounding its diphosphate moiety. Risedronate binds in essentially the same fashion and forms a hydrogen bond with a threonine deeper in the GPP site. The diphosphate part of IPP binds to FPPS via a series of salt bridge interactions with basic residues such as lysines, arginines and histidines. The active site appears more compact than in the avian crystal structure. It is not clear whether the *E. coli* and avian enzymes are simply different or if an induced fit movement closes the active site. If the two bisphosphonate molecules can form a three magnesium ion complex, similar strong interactions are likely to overcome the stabilization gained by one hydrogen bond in the GPP site.

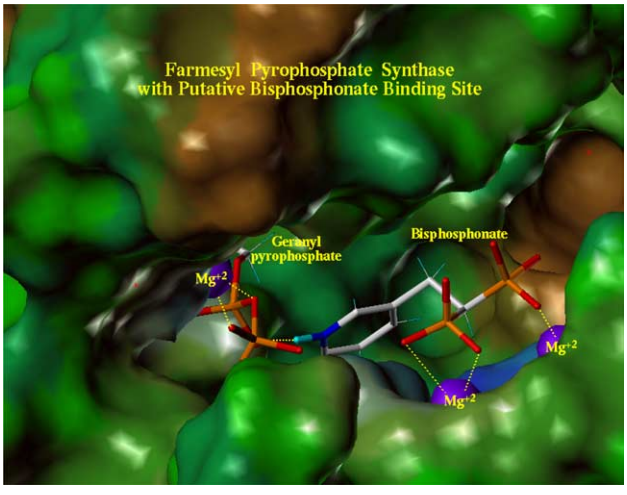

Fig. 2. A proposed bisphosphonate binding site in the avian farnesyl diphosphate synthase–GPP complex. The bisphosphonate risedronate is modeled adjacent to geranyl pyrophosphate which is found in the 1UBW X-ray structure.

Figs. 3A and B show the clustering of 50 docking runs for risedronate and NE-58051, respectively. The best runs for risedronate and NE-58051 (lowest energy) belonging to the main cluster are shown in Figs. 3C and D, respectively. Risedronate forms a salt bridge between its pyridinium hydrogen and two oxygens of the diphosphate moiety of GPP. The stabilization brought about by this electrostatic interaction clearly favors the binding of risedronate when a GPP molecule is present in the GPP site. No such stabilizing interaction can be found if the GPP site is empty.

NE-58051 is unable to form such interactions. Indeed, its nitrogen points away from the diphosphate moiety of GPP. Instead, we have found that its pyridinium ring can turn to form a hydrogen bond with tyrosine 188. This interaction is certainly much weaker than the salt bridge formed in the case of risedronate.

Next, we replaced the GPP molecule by a bisphosphonate inhibitor. Risedronate was manually docked in the GPP site on the basis of the complex observed in the *E. coli* structure. It is remarkable that although the first *E. coli* aspartate rich motif is DDxxxxD, the two aspartates binding the magnesium ions are in the same locations and conformations as in the avian structure. We constructed the FPPS-NE-58051 complex using the risedronate backbone as a guide. At this point, it was considered more important to monitor the interactions of the bisphosphonate moiety of NE-58051 than optimize its side chain orientation.

Fig. 4 shows the results of the docking experiments in the second site with the corresponding bisphosphonate molecule in the GPP site. Again, both inhibitors converged toward a unique docking conformation that is similar to the one observed with GPP in the GPP site.

Attempted docking experiments of N-BPs in the GPP site of FPPS with no other inhibitor or substrate present in this second site failed, with most docked molecules locating their side chains outside the DMAPP/GPP site even when the center of the site is chosen as the origin of the docking (results not shown). The driving forces behind such behavior are the available space in the open conformation of the enzyme, a lack of strong stabilizing

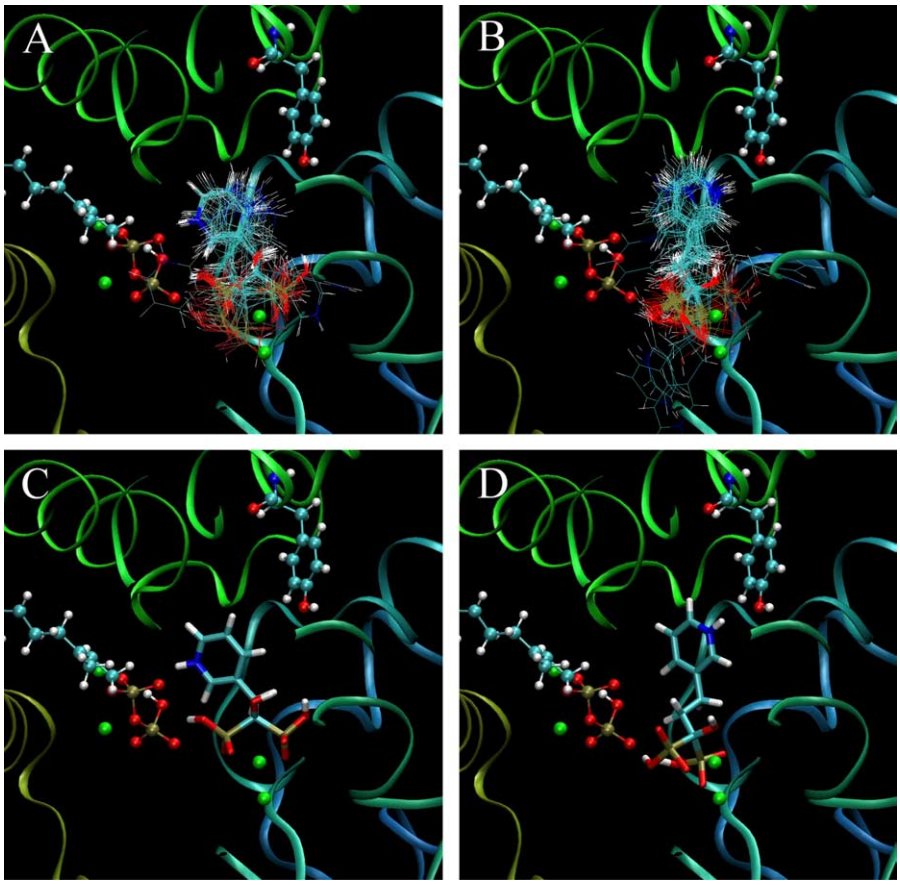

Fig. 3. Docking of risedronate and NE58051 in the second site with GPP in the GPP site. Enzyme backbone is represented in ribbon format, GPP, Mg^{2+} ions and aspartates are represented in ball and stick format. (A) 50 docking runs of risedronate represented in wire format. (B) 50 docking runs of NE58051 represented in wire format. (C) Best run of risedronate represented in licorice format. (D) Best run of NE58051 represented in licorice format.

interactions in the DMAPP/GPP site and some favorable interactions present in that open space (aspartates from the second DDxxD motif). In a recent paper [25], the Oldfield group obtained similar results while docking risedronate in the GPP site of the *E. coli* enzyme with no IPP present in the IPP site. We decided to dock the bisphosphonate in the GPP site with the second site already occupied by the inhibitor (Fig. 5).

Three binding modes were found for risedronate. The first one places the risedronate in an ideal position to form a salt bridge between the pyridinium and aspartate 169. The second binding mode of risedronate involves another salt bridge between the pyridinium and aspartate 259. The third binding mode allows the formation of a hydrogen bond with threonine 196 as seen in the *E. coli* X-ray structure.

The docking of NE-58051 produces two distinct binding modes. The first one allows the formation of a hydrogen bond between the pyridinium hydrogen and threonine 196. This binding mode is very similar to the one observed in the *E. coli*—risedronate complex. The second binding is stabilized by the nearby aspartate 169 and asparagine 260 side chains as well as the backbone oxygen of alanine 173 and proline 174.

It appears that docking a bisphosphonate into the GPP site never leads to a unique solution. If the bisphosphonate molecules bind to the GPP site in a unique fashion, the Autodock simulations were unable to identify it. This can be attributed to (i) the relatively large space available in this site meant to bind the large GPP molecule and (ii) the lack of a dominant interaction that forces the bisphosphonate into one position. However, it is significant that one of the preferred docked conformations is equivalent to the one observed in the *E. coli* X-ray crystal structure of FPPS.

2.3. FPPS inhibition assay results

Farnesyl pyrophosphate synthase catalyzes the condensation of geranyl pyrophosphate and isopentyl pyrophosphate to form farnesyl pyrophosphate and pyrophosphate [26,27]. As expected, the enzyme active site has two distinct binding sites that specifically bind one kind of substrate. We therefore performed prelimin-

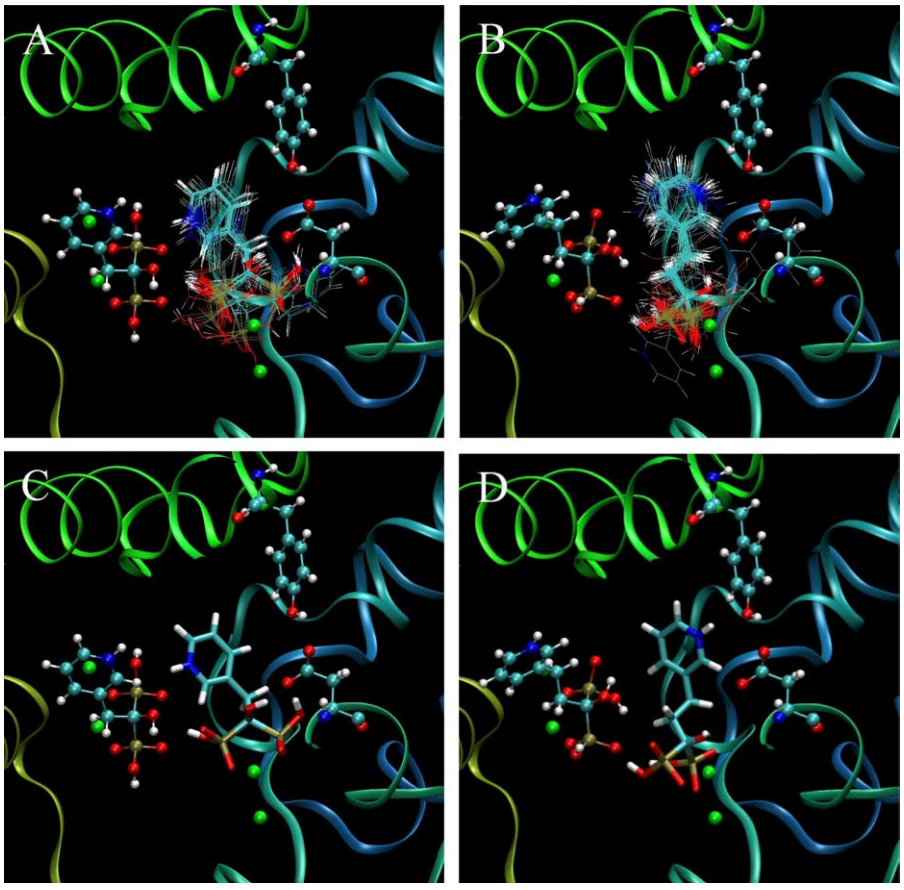

Fig. 4. Docking of risedronate and NE58051 in the second site with a second inhibitor in the GPP site. Enzyme backbone is represented in ribbon format, GPP, Mg^{2+} ions and aspartates are represented in ball and stick format. (A) 50 docking runs of risedronate represented in wire format. (B) 50 docking runs of NE58051 represented in wire format. (C) Best run of risedronate represented in licorice format. (D) Best run of NE58051 represented in licorice format.

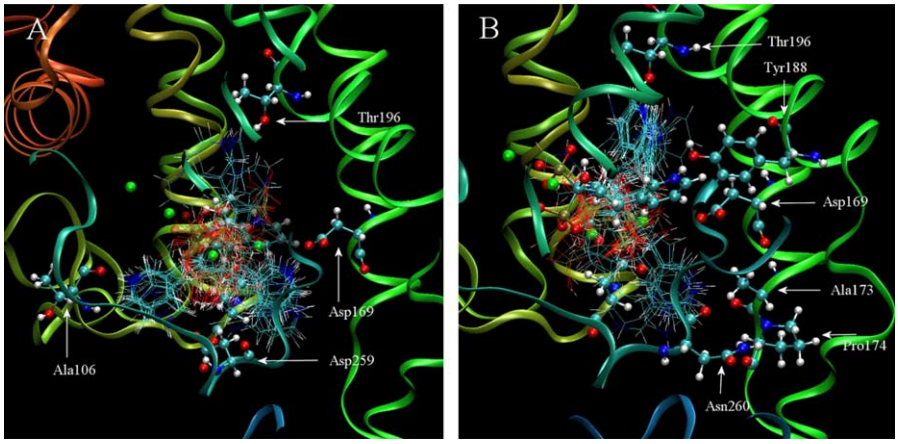

Fig. 5. Docking of risedronate and NE58051 in the GPP site with the best docked conformation of the same molecule in the second site. Enzyme is represented in ribbon format, inhibitors, Mg^{2+} ions and relevant residues are represented in ball and stick format. (A) 50 docking runs of risedronate represented in wire format. (B) 50 docking runs of NE58051 represented in wire format.

ary kinetic experiments to characterize the inhibition behavior of each substrate in the presence of varying concentrations of the other.

Lineweaver–Burk (LB) and Dixon plots of risedronate inhibition kinetic data are shown in Fig. 6 with either GPP (left) or IPP (right) as the variable substrate. Based on the LB plots, risedronate is a competitive inhibitor versus GPP and a non-competitive inhibitor versus IPP. However, the Ki values extracted from these LB plots are not constant. The apparent Ki of

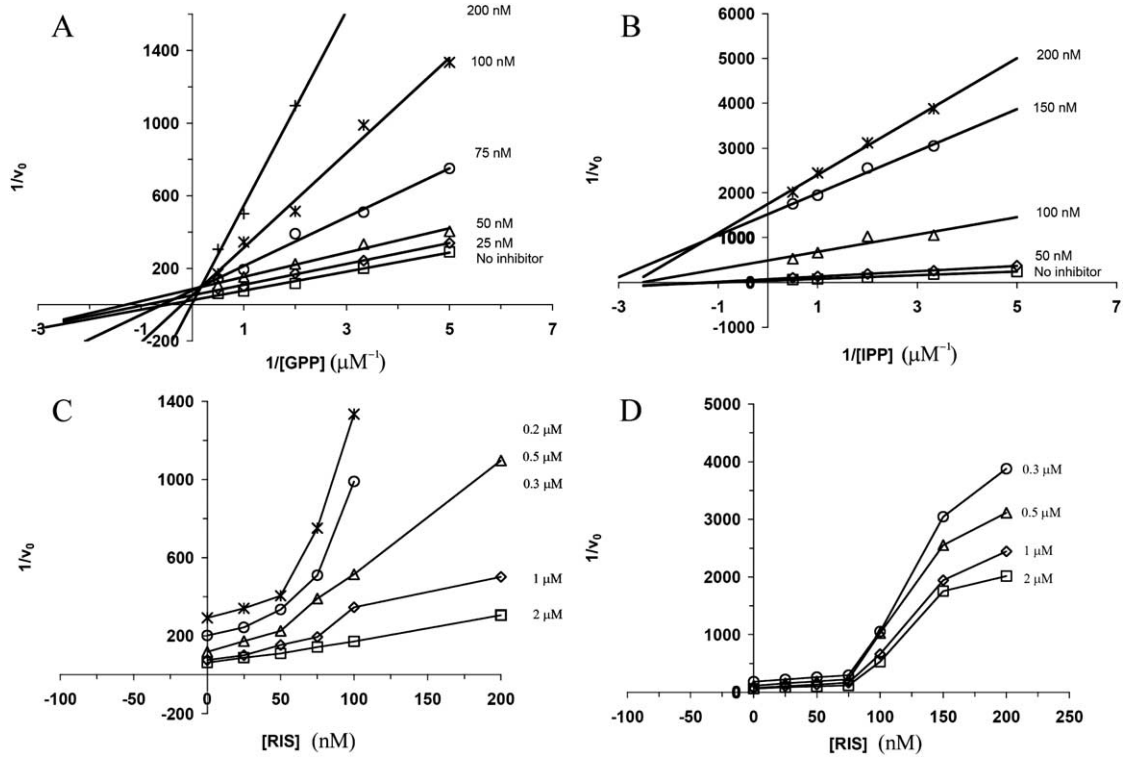

Fig. 6. Lineweaver–Burk plot of FPPS assays. (A) Risedronate inhibitor, GPP as the variable substrate [IPP] = 2 μM. (B) Risedronate inhibitor, IPP as the variable substrate [GPP] = 2 μM. Dixon plot of FPPS assays. (C) Risedronate inhibitor, GPP as the variable substrate [IPP] = 2 μM. (D) Risedronate inhibitor, IPP as the variable substrate [GPP] = 2 μM.

risedronate decreases as the inhibitor concentration increases. This nonclassical behavior is further illustrated by the non-linear Dixon plots obtained. When the IPP concentration is fixed and the GPP concentration is variable, the Dixon plot changes from linear at high GPP concentration to exponential at low GPP concentration. Furthermore, for all GPP concentrations tested, the Dixon plot initially shows a linear phase that shifts to an exponential phase at a particular (critical) risedronate concentration. This concentration of inhibitor is fairly independent of the GPP and IPP concentrations. When GPP concentration is variable, the critical risedronate concentration is 50 nM and when the IPP concentration is variable, the critical concentration is 75 nM.

Typically, this behavior is associated with a multi-site inhibition [28]. As stated above, FPPS catalyzes the condensation of two isoprenoid diphosphates, thus the enzyme must bind two pyrophosphate moieties. Bisphosphonates mimic the shape and electrostatic charge distribution of the pyrophosphate part of isoprenoid diphosphate substrates. It is therefore reasonable to postulate that two bisphosphonates bind simultaneously to the FPPS active site at inhibitor concentrations above a critical value, i.e., 50–75 nM for risedronate. It is remarkable that the in vitro inhibition of FPPS is markedly enhanced by the binding of a second inhibitor molecule. The known efficiency of this class of compounds for inhibition of FPPS could be a result of such multisite inhibition.

The Lineweaver–Burk and Dixon plots for NE-58051 inhibition kinetics are shown in Fig. 7 with either GPP (left) or IPP (right) as the variable. Similarly to risedronate, NE-58051 displays an apparent competitive inhibition with respect to GPP and noncompetitive inhibition with respect to IPP. However, the Dixon plots do not show the same marked exponential increase that occurs with risedronate. When GPP is the variable, a small curvature of the Dixon plot is found. With IPP as the variable, no exponential increase in inhibition is observed despite the much higher concentration of inhibitor used.

The lack of an exponential increase in inhibition by NE-58051, i.e., the inability of FPPS to bind two inhibitor molecules, correlates with its lesser inhibitory activity compared to risedronate.

In this work, we propose a hypothesis to rationalize differences in N-BP anti-resorptive activities using both theoretical and experimental approaches. Several caveats should be applied to these results.

1. We constructed a human homology model based on the available avian X-ray structures and postulated that two sets of magnesium ions bind to the two DDxxD aspartate-rich motifs of the enzyme. The

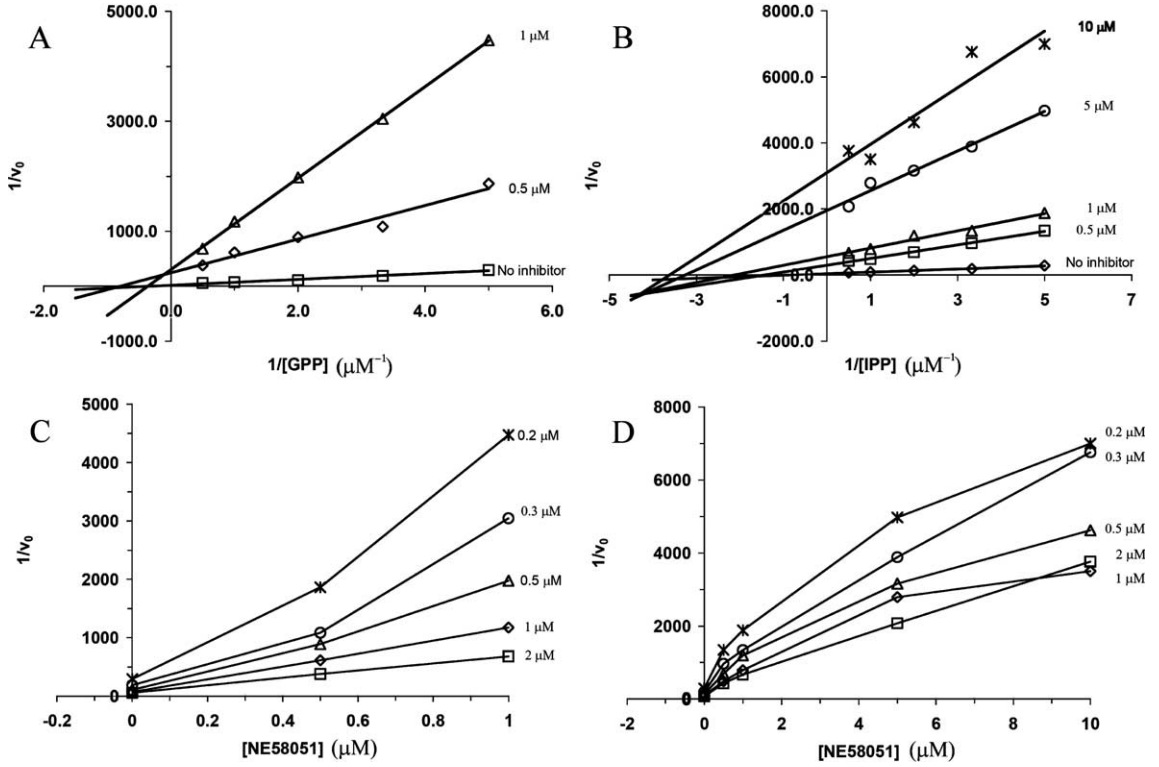

Fig. 7. Lineweaver–Burk plot of FPPS assays. (A) NE58051 inhibitor, GPP as the variable substrate [IPP] = 2 μM. (B) NE58051 inhibitor, IPP as the variable substrate [GPP] = 2 μM. Dixon plot of FPPS assays. (C) NE58051 inhibitor, GPP as the variable substrate [IPP] = 2 μM. (D) NE58051 inhibitor, IPP as the variable substrate [GPP] = 2 μM.

recently published X-ray structure of *E. coli* enzyme shows however different IPP and GPP binding sites. When available, the human FPPS crystal structure will determine the accuracy of the human homology model made here.

2. In the docking procedure, the enzyme is treated as a rigid body. Binding of one or two inhibitors to the enzyme may modify its conformation modulating active site properties. Induced fit binding structural effects can only be clearly demonstrated by X-ray crystallography or the use of biophysical methods.
3. As expected, we found that the binding energy is dominated by the electrostatic interaction between the bisphosphonate moiety and the magnesium ions. The energy of formation of this complex could not be precisely evaluated at the level of theory available.
4. It is known that FPPS is in fact a dimer [23]. What is not known is how the monomer subunits interact with each other. As a simplification, we implicitly assumed that the monomers are fairly independent. A recent report suggested some interaction between the subunits [29], proposing an intersubunit location of the active site. This hypothesis is not supported by the avian or *E. coli* X-ray results which indicate a separation of about 20 Å between intersubunit active sites. Nonetheless, allosteric interactions of the active site cannot be excluded.

3. Conclusion

Molecular modeling and enzyme inhibition studies suggest that binding of bisphosphonates to the GPP site does not distinguish between potent (risedronate) and nonpotent (NE-58051) N-BPs. This binding pocket can accommodate either DMAPP or GPP in two separate coupling steps catalyzed by FPPS. We therefore investigated the theoretical docking of two structurally similar N-BPs in a human recombinant FPPS site, reconstructed on the basis of similarity between both DDxxD motifs. This binding model could help explain the differences in the potency of N-BPs that has been observed with several pairs of active/inactive, structurally related analogs. A cooperative model, involving the binding of two molecules of N-BP to the FPPS enzyme, is a potential mode of inhibition that appears to be consistent with the data presented here. This cooperative binding requires the establishment of a salt bridge between the protonated nitrogen of one N-BP and a

phosphonate moiety of the other. The difference in the inhibitory potency of the two N-BPs evaluated in this work could be rationalized on the basis that risedronate satisfies the salt bridge requirement for the IPP binding site whereas NE-58051 does not.

Pending X-ray structural data for the actual human enzyme, the human homology model is the closest approximation available to provide insights into human FPPS—inhibitor interactions. Ultimately, validation of this approach will also depend on its usefulness in design of more potent FPPS N-BP inhibitors.

4. Experimental methodology

4.1. Expression of recombinant human FPP synthase

The human FPPS clone KIAA 1293 was obtained from the Kazusa DNA Research Institute, Japan. The coding region was cloned into the bacterial expression vector pBAD (InVitrogen) and expressed in *E. coli* TOP10f'. Bacterial cultures were inoculated with 20% by volume of an overnight bacterial culture in LB broth with 50 μg/ ml ampicillin at 37 °C with vigorous aeration. These cultures were grown for 2 h prior to induction with arabinose (0.02% w/v). After induction, the cultures were grown for an additional 5 h before harvesting by centrifugation at 7000*g* for 10 min.

4.2. Purification of FPP synthase

The bacterial pellet was resuspended in 5 ml per gram wet weight of ice cold homogenization buffer (100 mM potassium phosphate pH 7.0, 0.5 mM EDTA, 10 mM 2-mercaptoethanol + 50 μl protease inhibitors) and homogenized by sonication 3 times on medium power for 10 s on ice with a cooling period between each 10 s burst. The lysate was then centrifuged at 13,000*g* for 20 min at 4 °C. FPPS was purified to homogeneity by loading onto a DE53 column and eluting with a phosphate gradient (from 100 to 200 mM potassium phosphate, pH 7.0). The fractions containing FPP synthase activity were ammonium sulphate precipitated (0–70% fraction) and the redissolved pellet loaded onto a butyl agarose column. The enzyme was eluted with a gradient from 1 M ammonium sulphate, 10 mM potassium phosphate pH 7.0, to 10 mM potassium phosphate, pH 7.0. Fractions with FPP synthase activity were pooled and concentrated by dehydration using PEG6000. This fraction was loaded onto a hydroxyapatite column and eluted with a gradient from 10 mM Tris/HCl pH 7.0 to 60 mM potassium phosphate, 10 mM Tris/HCl pH 7.0. All fractions containing pure enzyme were pooled. All buffers contained 10 mM 2-mercaptoethanol.

4.3. FPP synthase assay

FPP synthase was assayed by the method of Reed and Rilling [23] with modifications. For kinetic analysis 40 ng of pure FPP synthase were assayed in a final volume of 100 μl buffer containing 50 mM Tris pH 7.7, 2 mM $MgCl_2$, 0.5 mM DTT. To investigate the effect of variable concentrations of GPP, IPP concentration was at 2 μM (^{14}C-IPP, 400KBq/μM) with varying concentrations of GPP as described. To investigate the effect of variable IPP, GPP concentration was 2 μM and IPP was varied as described. Reactions also contained the appropriate concentration of N-BP. Reactions were started with the addition of enzyme and allowed to proceed for an appropriate period of time at 37 °C. Reactions were timed such that a maximum of 15% of the available substrate was used. Assays were terminated by the addition of 0.2 ml of concentrated HCl:methanol (1:4) and further incubated for 10 min at 37 °C. The reactions were then extracted with 1 ml of ligroin, thoroughly mixed and briefly centrifuged. The amount of radioactivity in the upper phase was determined by mixing 0.5 ml of the ligroin with 4 ml of general purpose scintillant. This solution was then counted using a Packard Tricarb 1900CA scintillation counter. Enzyme velocity is expressed as μM of FPP/min/pmol enzyme.

4.4. Human homology model of FPPS

The 3D structure of human FPPS was constructed by the SWISS-MODEL server [30] with the avian structures [31,32] as a template. A sequence comparison of human FPPS and avian FPPS has 66.2% identity with no gaps or inserts, so an automated homology model seemed feasible. While the avian FPPS structure lacks the first nineteen residues, the predicted human FPPS structure lacks only the first five residues, because the avian sequence is longer than the human. These missing residues are not part of the active site and should have no bearing on the docking studies. Inspection of the active site of the human model showed the active sites open and accessible for docking studies. Further, a comparison with the active site of the *E. coli* FPPS complex with risedronate showed a similar network of residues surrounding both active sites in the human model.

4.5. Molecular docking

Quantum mechanical calculations were performed with GAUSSIAN '03 [33]. Docking experiments were carried out using the Autodock 3.05 program suite [34]. The figures were prepared with VMD [35]. Bisphosphonate molecules were partially optimized with the B3LYP functional and 6–31G* basis set. Some dihedral angles were restrained in order to prevent the molecule from collapsing in the gas phase calculation. To avoid a

hydrogen transfer from nitrogen to phosphonate group, the dianionic species having one hydrogen per phosphonate group and a neutral amine were used for calculation. After optimization, a hydrogen was added to the nitrogen and the charges were calculated by single point calculation at the B3LYP/6-311+G** level. The protein was prepared with the standard protonation state: histidines, lysines, and arginines were protonated, glutamate and aspartate residues were deprotonated. When docking N-BPs in the GPP site, Thr196 was turned by 60 degrees to orient its hydroxyl group toward the binding site as seen in the *E. coli* X-ray crystal structure. Amber partial charges for the enzyme were assigned by *q. amber* and solvation parameters for the enzyme were determined by *addsol 3.0* from the Autodock suite. Magnesium charges were set to +2. The receptor comprised the enzyme, two magnesium ions, and a GPP or bisphosphonate in either GPP or IPP binding sites. Rotatable bonds were assigned to the ligand using *Autotors 3.05* (all cycles are constrained rigid). The grid map contains 120 points in each direction spaced by 0.2 Å. The grid spans over 24 Å in each direction center in the binding site of interest. A Lamarckian genetic algorithm was employed, with a mutation rate of 0.02 and a crossover rate of 0.8. Only the lowest binding energy (most negative) out of ten generations survives. Fifty runs per molecule were carried out with a maximum of 1,500,000 energy evaluations per run. The resulting structures were clustered with a RMSD tolerance of 1 Å. The results were visualized with VMD.

Acknowledgments

The authors thank Procter & Gamble Pharmaceuticals, Inc. for financial support.

References

[1] G.A. Rodan, J. Bone. Miner. Res. 17 (2002) N150.
[2] R.G. Russell, M.J. Rogers, Bone 25 (1999) 97.
[3] (a) O. Bijvoet, Bisphosphonate on bones, Elsevier Science, Amsterdam, 1995;
(b) H. Fleisch, Bisphoshonates in Bone Disease, fourth ed., Academic Press, San Diego, 2000.
[4] J.R. Green, M.J. Rogers, Drug Dev. Res. 55 (2002) 210.
[5] F.H. Ebetino, M.D. Francis, M.J. Rogers, R.G.G. Russell, Rev. Contemp. Pharmacother. 9 (1998) 233.
[6] E.R. Van Beek, C.W.G.M. Lowik, F.H. Ebetino, S.E. Papapoulos, Bone 23 (1998) 437.
[7] G.H. Nancollas, R. Tang, S. Gulde, F.H. Ebetino, R.J. Phipps, R.G.G. Russell, J. Bone Miner. Res. 17 (2002) s36.
[8] J.E. Dunford, K. Thompson, F.P. Coxon, S.P. Luckman, F.M. Hahn, C.D. Poulter, F.H. Ebetino, M.J. Rogers, J. Pharmacol. Exp. Ther. 296 (2001) 235.
[9] J.D. Bergstrom, R.G. Bostedor, P.J. Masarachia, A.A. Reszka, G. Rodan, Arch. Biochem. Biophys. 373 (2000) 231.
[10] C.M. Szabo, M.B. Martin, E. Oldfield, J. Med. Chem. 45 (2002) 2894.
[11] M.B. Martin, J.S. Grimley, J.C. Lewis, H.T. Heath III, B.N. Bailey, H. Kendrick, V. Yardley, A. Caldera, R. Lira, J.A. Urbina, S.N.J. Moreno, R. Docampo, S.L. Croft, E. Oldfield, J. Med. Chem. 44 (2001) 909.
[12] J.M. Sanders, A.O. Gomez, J. Mao, G.A. Meints, E.M. Van Brussel, A. Burzynska, P. Kafarski, D. Gonzalez-Pacanowska, E. Oldfield, J. Med. Chem. 46 (2003) 5171.
[13] M.B. Martin, W. Arnold, H.T. Heath III, J.A. Urbina, E. Oldfield, Biochem. Biophys. Res. Commun. 263 (1999) 754.
[14] F.H. Ebetino, M.J. Rogers, J.E. Dunford, X. Liu, R. Phipps, R.G.G. Russell, G. Mieling, B. Barnett, J. Bone Miner. Res. 17 (Suppl. 1) (2002) s256.
[15] D.J. Hosfield, Y. Zhang, D.R. Dougan, A. Broun, L.W. Tari, R.V. Swanson, J. Finn, J. Biol. Chem. 279 (2004) 8526.
[16] F.H. Ebetino, A.V. Bayless, J. Amburgey, K.J. Ibbotson, S. Dansereau, A. Ebrahimpour, Phosphorus, Sulfur Silicon Relat. Elem. 109–110 (1996) 217.
[17] E.R. Van Beek, L.H. Cohen, I.M. Leroy, F.H. Ebetino, C.W.G.M. Lowik, S.E. Papapoulos, Bone 33 (2003) 805.
[18] A. Montalvetti, A. Fernandez, J.M. Sanders, S. Ghosh, E. Van Brussel, E. Oldfield, R. Docampo, J. Biol. Chem. 278 (2003) 17075.
[19] A. Montalvetti, B.N. Bailey, M.B. Martin, G.W. Severin, E. Oldfield, R. Docampo, J. Biol. Chem. 276 (2001) 33930.
[20] C.M. Szabo, Y. Matsumura, S. Fukura, M.B. Martin, J.M. Sanders, S. Sengupta, J.A. Cieslak, T.C. Loftus, C.R. Lea, H.-J. Lee, A. Koohang, R.M. Coates, H. Sagami, E. Oldfield, J. Med. Chem. 45 (2002) 2185.
[21] E. Kotsikorou, E. Oldfield, J. Med. Chem. 46 (2003) 2932.
[22] V.D. Ding, B.T. Sheares, J.D. Bergstrom, M.M. Ponpipom, L.B. Perez, C.D. Poulter, Biochem. J. 275 (1991) 61.
[23] B.C. Reed, H.C. Rilling, Biochemistry 14 (1975) 50.
[24] L.J. Hyland, T.A. Tomaszek Jr., T.D. Meek, Biochemistry 30 (1991) 8454.
[25] F. Cheng, E. Oldfield, J. Med. Chem. 47 (2004) 5149.
[26] K. Ogura, T. Koyama, Chem. Rev. 98 (1998) 1263.
[27] P.-H. Liang, T.-P. Ko, A.H.J. Wang, Eur. J. Biochem. 269 (2002) 3339.
[28] I.H. Segel, Enzyme Kinetics: Behavior and Analysis of Rapid Equilibrium and Steady-state Enzyme Systems, Wiley Interscience, New York, 1993.
[29] T. Koyama, Y. Gotoh, T. Nishino, Biochemistry 39 (2000) 463.
[30] T. Schwede, J. Kopp, N. Guex, M.C. Peitsch, Nucleic. Acids. Res. 31 (2003) 3381.
[31] L.C. Tarshis, P.J. Proteau, B.A. Kellogg, J.C. Sacchettini, C.D. Poulter, Proc. Natl. Acad. Sci. USA 93 (1996) 15018.
[32] L.C. Tarshis, M. Yan, C.D. Poulter, J.C. Sacchettini, Biochemistry 33 (1994) 10871.
[33] M.J. Frisch, et al., Gaussian, Inc., Pittsburgh, PA, 2003.
[34] G.M. Morris, D.S. Goodsell, R.S. Halliday, R. Huey, W.E. Hart, R.K. Belew, A.J. Olson, J. Comput. Chem. 19 (1998) 1639.
[35] W. Humphrey, A. Dalke, K. Schulten, J. Mol. Graph. 14 (1996) 33.